Student thesis series INES nr 481

Modelling the effects of land cover and climate change on watershed hydrology in south-western Ethiopia

Nicklas Thorlund Simonsen

2019
Department of
Physical Geography and Ecosystem Science
Lund University
Sölvegatan 12
S-223 62 Lund
Sweden

Nicklas Thorlund Simonsen (2019).
Modelling the effects of land cover and climate change on watershed hydrology in south-western Ethiopia
Bachelor degree thesis, 15 credits in *Physical Geography and Ecosystem Science*
Department of Physical Geography and Ecosystem Science, Lund University

Level: Bachelor of Science (BSc)
Course duration: *March* 2019 until *June* 2019

Modelling the effects of land cover and climate change on watershed hydrology in south-western Ethiopia

---

Nicklas Thorlund Simonsen

Bachelor thesis, 15 credits, in *Physical Geography and Ecosystem Science*

Supervisor:
Harry Lankreijer

Exam committee:
Dan Metcalfe
Marko Scholze

Abstract

Degradation of the hydrological regime is a pressing issue in the Ethiopian Highlands. It is one of the most rapidly degrading landscapes due to its topography and large amounts of annual precipitation. This problem has been exacerbated through anthropogenic influence from land use/land cover (LULC) and climate change. This paper presents the effect on the hydrological cycle caused by these changes through modelling the observed and projected changes between 1989-2079 in a watershed in South-Western Ethiopia. The Soil & Water Assessment Tool (SWAT) was used to quantify the changes in water quality and quantity. The model output showed a general increase in precipitation and temperature throughout the whole study period with an intensification of the secondary wet season. This caused an overall increase in the fluxes of the hydrological cycle and sediment yields for observed and projected years. The climactic changes to the watershed were accompanied by a strong anthropogenic influence on the LULC, which resulted in large increases to both surface runoff and sediment yield. The changes in LULC were shown have far greater impact on the hydrological regime than climate change alone. These findings indicate a need for intervention on a local scale to diminish further deterioration of the watershed.

Key words: *hydrological model, Soil & Water Assessment Tool (SWAT), land use/land cover (LULC), climate change, erosion, Ethiopian Highlands.*

Table of Contents

List of Abbreviations

SWAT: Soil & Water Assessment Tool

Physical features

CFRG: Coarse Fragment Factor

GCM: General Circulation Model

(G)DEM: (Global) Digital Elevation Model

HRU: Hydrological Response Unit

LULC: Land Use and Land Cover

(M)USLE: (Modified) Universal Soil Loss Equation

(P)ET: (Potential) Evapotranspiration

SCS-CN : Soil Conservation Service Curve Number

SNNR: Southern Nations, Nationalities, and People's Region

Datasets

ASTER: Advanced Spaceborne Thermal Emission and Reflection Radiometer

CFSR: Climate Forecast System Reanalysis

CMIP5: Coupled Model Intercomparison Project 5

HWSD: Harmonized World Soil Database

Government bodies

ESA: European Space Agency

FAO: Food and Agriculture Organization of the United Nations

USGS: United States Geological Survey

Introduction

Anthropogenic land surface changes have reached an unprecedented pace and magnitude as a result of growing demands from an expanding population (Lambin et al. 2001; Setegn et al. 2008; Sewnet and Abebe 2018; Kidane et al. 2019). In the last 50 years, the population of Ethiopia has increased from 22 million to over 100 million as of 2017 (The World Bank 2017). This has led to a large-scale conversion of the natural vegetation to pasture and cropland and put pressure on the environment to sustain such a rapidly growing population (Hurni 1988; Nyssen et al. 2004; Moges and Holden 2009; Sewnet and Abebe 2018; Bekele et al. 2019a). The environmental stress has resulted in extensive degradation and a change in the fluxes of the hydrological cycle (Gessesse et al. 2015; Alemneh et al. 2019; Permatasari et al. 2019), which often exacerbate the rate of degradation through increased erosion and runoff (Sajikumar and Remya 2015). Changes in climate may further intensify this process through alteration of the hydrological cycle (Bronstert et al. 2002; Bekele et al. 2019b).

The city of Sawla and the surrounding watershed lies in the south-western Ethiopian highlands, which is one of the most rapidly degrading environments due to the accelerated soil erosion by water (Hurni 1988; Nyssen et al. 2004; Gessesse et al. 2015; Addis et al. 2016; Adimassu et al. 2019; Alemneh et al. 2019). The highlands experience large quantities of annual precipitation, which coupled with steep slopes and extensive cultivation leads to high rates of erosion (Nyssen et al. 2004; Setegn et al. 2008). National soil-erosion assessments reveal that nearly half of the highlands in the country are significantly eroded and roughly 3% of them are degraded beyond restoration (Gessesse et al. 2015). This can largely be attributed to the conversion of natural vegetation like forests, shrubland, and grassland to cultivation and pasture (Hurni 1988; Moges and Holden 2009; Alemneh et al. 2019). The highlands have been under anthropogenic influence for a long time, but the rate of population growth has caused people to increasingly cultivate steeper slopes (Hurni 1988; Nyssen et al. 2004).

Climate change is likely to affect the fluxes in the hydrological cycle, such as runoff, lateral flow, and groundwater flow, by altering mean states and variabilities (Bronstert et al. 2002; Bekele et al. 2019b). Climate projections for Ethiopia indicate an overall increase in temperature and precipitation for all months, but especially within the wet season (The World Bank 2019). This may lead to larger variations in the temporal distribution of precipitation events and the intensity thereof. Higher intensity rainfall events can lead to extreme events of runoff and sediment detachment, which may exaggerate the rate of degradation in the highlands (Bronstert et al. 2002).

In order to mitigate the effects of land use/land cover (LULC) and climate change on the watershed hydrology, it is important to understand how each aspect affects the other. This is commonly done by measuring changes in field, but this can be both time consuming and costly and, in some areas, impossible. Modelling provides a good alternative to direct measurements as it has the capabilities to account for numerous parameters and make estimations about the future. Models also have the capability to give insight into underlying processes to facilitate a more detailed analysis of both causes and consequences. However, in order to provide accurate estimations about the watershed hydrology, models need to be calibrated and validated using in situ streamflow data. Stream gauges are unfortunately limited to a few key river basins in Ethiopia although the need for validated projections extend far beyond these areas (Mekonnen et al. 2009; Van Griensven et al. 2012; Addis et al. 2016). This study focuses on a watershed in the highlands of south-western Ethiopia that has not been previously investigated. Although results cannot be validated from stream flow gauges, they are presented as preliminary to assess the impact of anthropogenic influence on the ecosystem from a hydrological perspective. This study thus aims to investigate the how changes in LULC and climate affects the watershed hydrology using the SWAT 2012 (Soil & Water Assessment Tool) model.

The SWAT model was developed by the Texas Water Resource Institute at the Texas A&M University in Temple, Texas, USA. It is a river basin model used to compute hydrology, crop growth, pesticide transport, and carbon cycling among other land- and ecosystem aspects (Arnold et al. 2012b). The model was chosen for this study due to its efficient computing; comprehensive watershed analysis; and long history of validated studies both in- and outside the region of interest. Due to the scope of this study, the primary focus will be on the computing the land-based hydrology within the watershed. To provide estimations about the hydrological regime, the SWAT model requires a LULC characterization; a soil database; and a range of climate variables, which are all available through open-source projects.

Study area

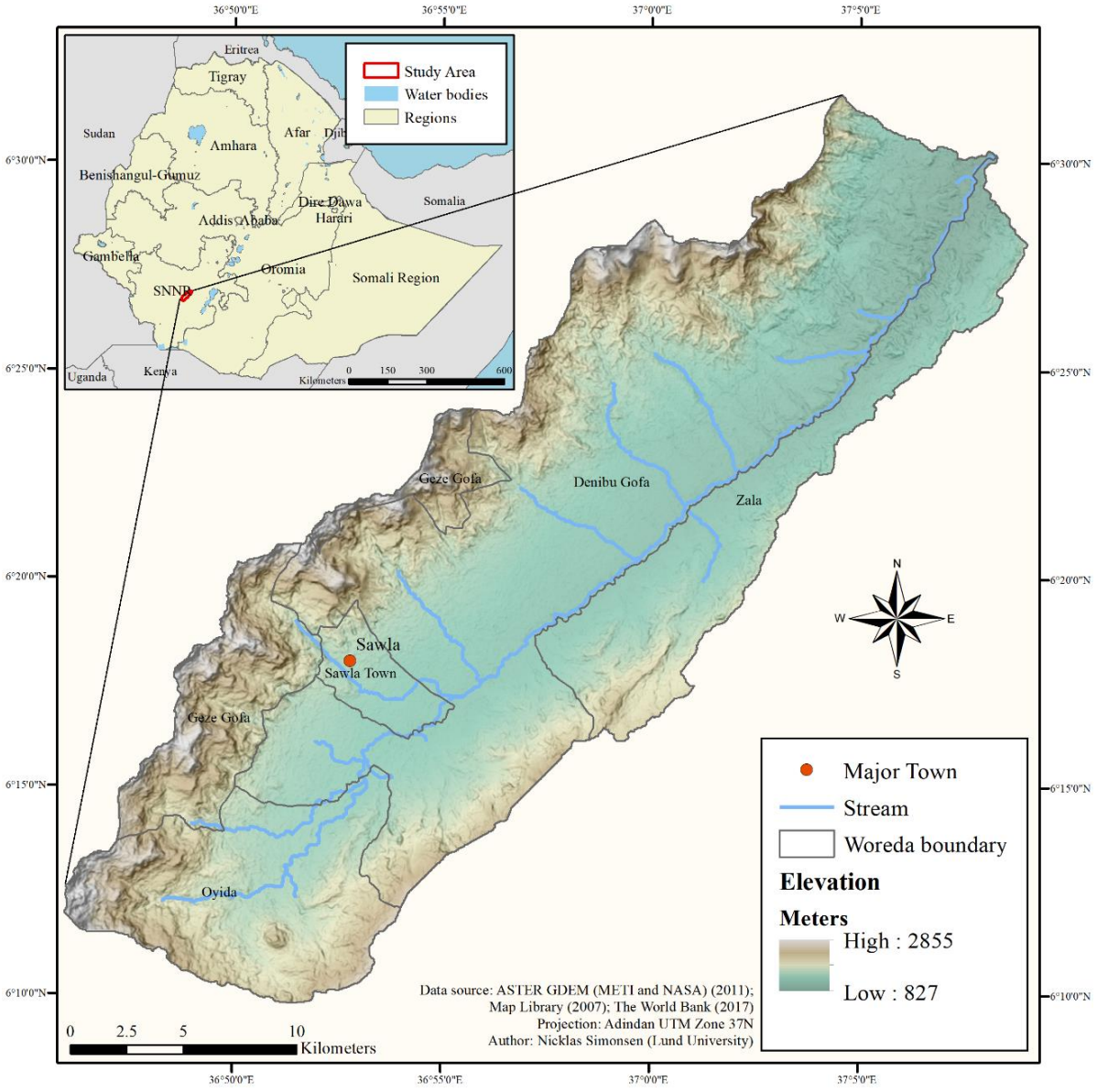

Figure 1: A shaded relief map of the study area, showing its location within Ethiopia and the general topography. Woredas (third-level division) demarcate the administrative borders within the watershed.

The Sawla watershed (639.5 km^2) is located between 6°10'00"-6°35'00"N and 36°45'00"-37°10'00"E in the region of Southern Nations, Nationalities, and People's Region (SNNR) in south-western Ethiopia (figure 1). It is divided between 5 different woredas (third-level administrative boundary) with the primary town, Sawla, being its own administrative boundary. The town experienced a growth from 15,764 to 22,704 people between 1994 and 2007 (Central Statistical Authority 1996; Central Statistical Agency 2007).

The topography is characterized by a large floodplain dominated by agriculture at the base of a steep ridge demarcating the watershed. The physiography of the watershed reveals elevation ranges

between 827-1375m in the floodplain to 2855m at the peaks surrounding it on the northern side and 2300m in the south. The soils found in the study area are Lithic Leptosols (4%), Humic Nitisols (41%), Humic Alisols (26%), and Dystric Leptosols (29%), with clay soils found predominantly in the floodplain and sandy clay loams on the slopes and plateaus (FAO/IIASA/ISRIC/ISS-CAS/JRC 2012). The Sawla watershed experiences two separate wet seasons; one very pronounced during spring and a lesser one during autumn due to the Intertropical Convergence Zone (ITCZ) oscillations. Records from the Climate Forecast Reanalysis System (CFSR) show average annual precipitation of 1700mm between 1989 and 2013 with maximum daily precipitation up to 30mm between 1989 and 2013. The south-western area of the watershed receives the most precipitation and decreases gradually towards the north-east. Due to the grid size of the CFSR dataset, no clear relationship between elevation and precipitation can be drawn. Mean annual maximum and minimum temperatures for the same period are 33° and 13° respectively.

Methodology

Data collection

Satellite imagery and digital elevation model

The LULC was classified using satellite imagery from Landsat 4-5 TM from United States Geological Survey (USGS 1989) and Sentinel-2 from the European Space Agency (ESA) (Copernicus Sentinel data 2019). The Landsat 4-5 TM images are produced at a resolution of 30 meters in 7 bands and the images taken by Sentinel-2 are available at a resolution of 10 meters in 13 bands. The satellite images were taken during March 1 and 23 for the years 1989 and 2019, respectively. This period was used due to relatively cloud free conditions and the large spectral distinction between cultivated and natural vegetation leading up to the rain season. The digital elevation model (DEM) was extracted from the 30-meter resolution Advanced Spaceborne Thermal Emission and Reflection Radiometer (ASTER) dataset (USGS 2011).

Soil data

The Harmonised World Soil Database 1.2 (HWSD) by the Food and Agriculture Organization of the United Nations (FAO/IIASA/ISRIC/ISS-CAS/JRC 2012) was used to estimate most of the hydrologic variables pertaining to the soil of the watershed. The HWSD is a global raster soil database with a resolution of 30 arc-seconds and contains a large amount of information about each soil types. However, some attributes necessary to run the SWAT analysis were unspecified in the soil database

and were instead estimated using similar soils existing in the SWAT soil database. Attributes included in the soil database are listed in table A1 and A2 (appendix A).

Climate data

The Climate Forecast System Reanalysis (CFSR) by National Centers for Environmental Prediction (NCEP) was used to determine climactic variables within the watershed due to a lack of consistent data from weather stations in the area. The values used to run the model were collected daily over a 25-year period between 1989-2013 and was used to simulate climate/weather for both study periods. The spatial resolution of each grid cell was 18.7 arc-minutes or approximately 33km from 6°5'16.8"N-6°42'46.8"N and 36°52'30"-37°30'0"E. All variables were interpolated between the centroids to find the most representative values for the watershed. A linear regression was fitted between all the years to derive an equation for estimating values in 1989 and 2019. The modelled parameters for 2049 and 2079 used an average value estimated from 16 model projections under the RCP 8.5 scenario as part of the Coupled Model Intercomparison Project 5 (CMIP5) program. The two projections used mean values between the years 2040-2059 and 2070-2079 to estimate changes in precipitation, rainfall intensity, and temperature over the watershed. The difference in spread between the two means is caused by the output of the models used, which used intervals of 20 years. Additional climate parameters, which had not been projected by the General Circulation Models (GCM), such as wind speed; solar radiation; and relative humidity were estimated from the initial 25-year mean by fitted regressions. Climate parameters included in the model are shown in table A3 and A4 (appendix A).

Data analysis – LULC

The LULC was classified using manual digitization in ArcGIS (ESRI 2016. ArcGIS Desktop: Release 10.5. Redlands, CA: Environmental Systems Research Institute) due to the relatively small rural settlements, which under unsupervised classification went undetected. A false colour composite (FCC) was created for both years in addition to a wetness and brightness index to aid in the detection of vegetation classes. The smallest unit was set to 20 ha for 2019 and 40 ha for 1989 due to the difference in cell sizes of the original satellite images. Only the LULC between 1989 and 2019 was quantified and included in the model. The LULC for the two projections (2049 and 2079) was assumed unchanged from the characterization in 2019 as the scope of this study did not include future LULC modelling.

LULC was classified according to the generic predefined classes of the SWAT model (table 1) with the addition of clouds for areas unclassifiable beneath them. The areas under the clouds were later subtracted before initiating the model. For the classification of LULC, a total of 9 classes were used (excluding clouds) in three major categories: agricultural areas; natural vegetation; and built-up areas (table 1). No water bodies were identified, and streams were aggregated to their nearest neighbour. The streams were later delineated using the SWAT toolset, ArcSWAT (Blackland Research & Extension Center 2018. ArcSWAT Desktop: Release 2012.10.21. Temple, TX: USDA Agricultural Research Service), in ArcGIS to ensure proper functionality when running the model. Areas of natural vegetation were classified from their spectral signature, while areas of agriculture were classified using geometry to distinguish them from natural vegetation and spectral reflection to differentiate between cultivation and pasture. Built-up areas were classified from a combination of spectral reflection and geometry and ranked using the width and material of the road and the clustering of houses within the settlements (table 1).

Vegetation type and management practices were not considered for cultivated areas due to the coarse imagery from the Landsat satellite. These features were also not identified in the Sentinel dataset for continuity's sake and thus all plots of cultivation are assumed homogenous. Parameters for built-up areas were modified from the SWAT database to fit the rural settlements of Ethiopia in terms of permeability and curb density. These modifications were estimated from the satellite images in 2019 by counting the length and fractional area of paved and unpaved roads in settlements.

Table 1: The LULC classes identified from the satellite imagery and used in the SWAT analysis. Spectral/geometric signature describe their appearance from satellite imagery using NDVI.

Code	LULC description	Major category	Spectral/geometric signature (FCC)
1	Bare soil	Natural Vegetation	Dark green or brown
2	Cultivated area	Agricultural areas	Green with distinct borders; or green/brown and terraced
3	Pasture	Agricultural areas	Light red/pink with distinct borders
4	Grassland	Natural vegetation	Light red/pink
5	Bush/shrubland	Natural vegetation	Patchy red dots on a pink or brown surface
6	Forest	Natural vegetation	Bright red
7	Low-density settlement	Built-up areas	White specks surrounded by red; few narrow dirt roads
8	Medium/low-density settlement	Built-up areas	White dots and red patches; dirt roads

9	Medium-density settlement	Built-up areas	White/grey with red dots; paved roads
10	Clouds		White

A confusion matrix was used to measure the level of classification errors in the LULC of 2019. The Google Earth Pro engine (Google Earth Pro 2019. Google Earth Pro Desktop: Release 7.3.2.5776. Mountain View, CA: Google) was used as ground truth to verify the classification due to a lack of in situ data and superior spatial resolution over the Sentinel-2 dataset. The images from Google Earth Pro (Google 2018) were recorded between 2017 and 2019 from December to January, and are thus within the same dry season as both study periods. Errors in the Landsat imagery were not quantifiable due to a lack ground truth through either better satellite imagery or field inventory records.

Slope

The ASTER GDEM was used to delineate the stream network, create sub-basins, and create the slope layer from the ArcSWAT toolset. The slope classification tool within ArcSWAT allows for a maximum of 5 distinct slope classes, which were defined in intervals of 10% ranging from 0-40% and above (figure 2).

Data analysis – SWAT

The SWAT-model is a comprehensive tool able to estimate hydrological coefficients due to the inclusion of an array of indirect parameters, such as management practices, nutrient cycling, vegetation types, etc. However, from the basic data available for the area and a lack of calibration and validation data, only a rough estimation of the hydrological output for the watershed is presented. As there are no lakes or reservoirs within the watershed the focus will be on the land phase processes. Hence only the necessary parameters required to run the model are explained below.

The 639.5 km^2 watershed was discretized into 29 sub-basins containing a total of 155 hydrological response units (HRU) in 1989 and 129 from 2019-2079. Each HRU was computed from a unique combination of slope class; LULC; and soil type (figure 2). In order to reduce the amount of unique HRUs, each class was aggregated at the recommended thresholds defined by Strauch et al. (2015) at 20%, 10%, and 20%, respectively. As a result, any LULC class, soil type, and slope class occupying less than the given fraction of the total watershed have been excluded. This step was done to ensure efficient simulations and to reduce complexity of the model.

Weather in the watershed was simulated using the built-in weather generator in SWAT, which used the input from 16 CFSR grid cells to interpolate values between the points. Weather data was

calculated on a daily time-step using average monthly values and standard deviation. Additionally, precipitation also used skew and probability of wet/dry days to simulate daily weather.

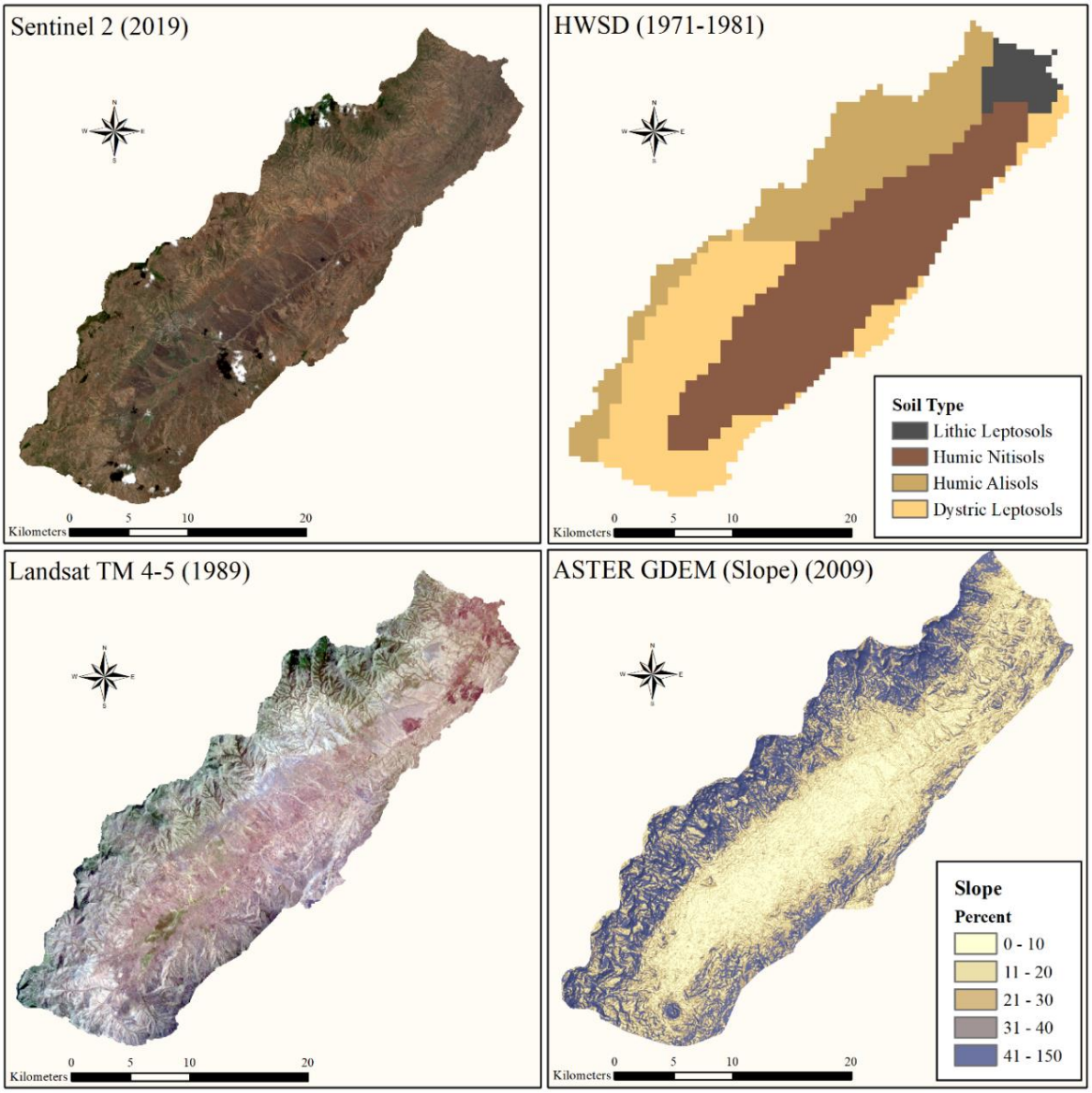

Figure 2: The layers constituting the HRU definitions. The Sentinel 2 and Landsat 4-5 TM data is shown as raw satellite images but have been classified before defining the HRU. The HWSD (Harmonised World Soil Database) shows the four soil types in the study area, and the ASTER GDEM image shows the slope (range) within the watershed.

The water balance of individual HRUs were used to evaluate the impact of changes in LULC, soil, and climate. Each unit is the function of:

$$SW_i = SW_{i-1} + R_i - Q_{sur,i} - E_{a,i} - w_{prc,i} - Q_{grw,i} \quad (1)$$

where i denotes the day, SW is the soil water content (mm), R is the amount of precipitation (mm), Q_{sur} is the surface runoff (mm), E_a is the amount of evapotranspiration (mm), w_{prc} is the amount of

water percolating into the vadose zone (mm), and Q_{grw} is the amount of return flow (mm) (Mekonnen et al. 2009). This balance is illustrated by Arnold et al. (1993) in figure 3.

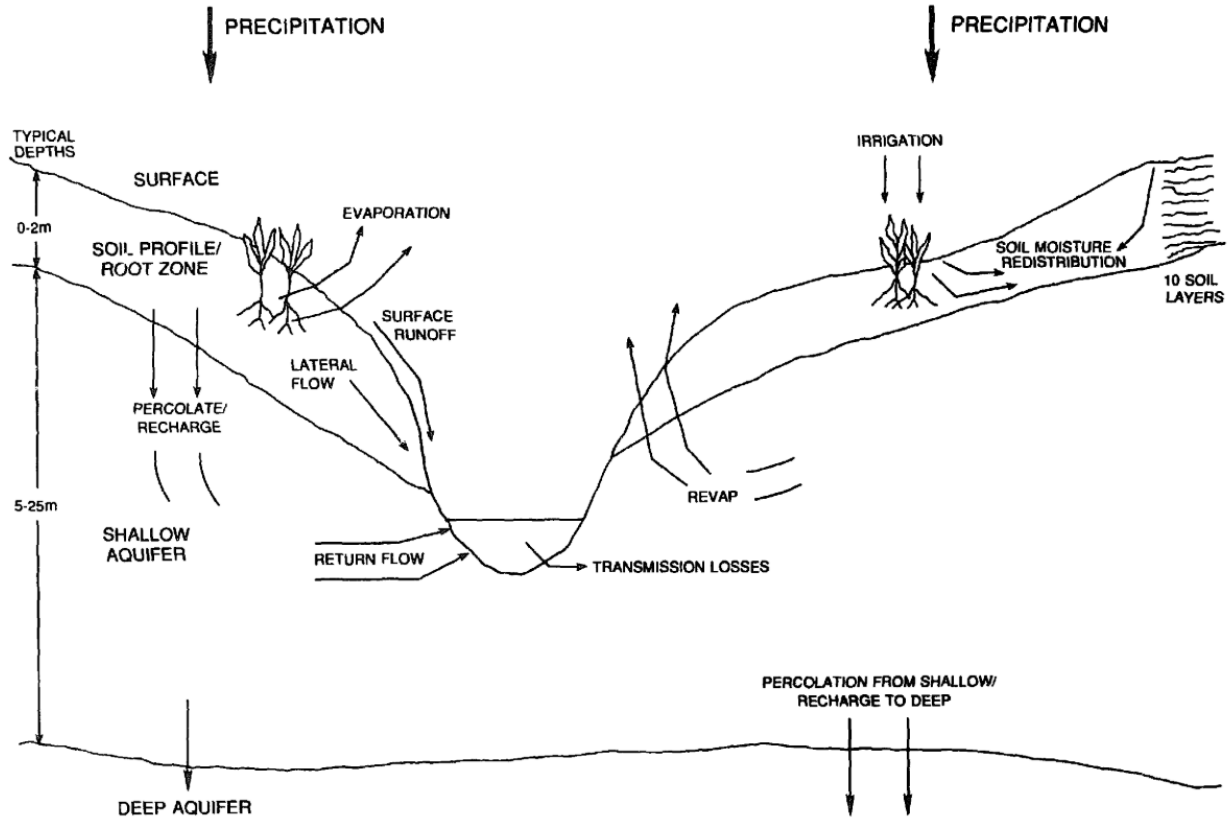

Figure 3: Illustrated hydrological balance used in the SWAT model. Illustration by Arnold et al. (1993).

Surface runoff

The surface runoff is calculated from the Soil Conservation Service (SCS) curve number procedure:

$$Q_{sur} = \frac{\left(R_{day} - I_a\right)^2}{\left(R_{day} - I_a + S\right)} \quad (2)$$

where Q_{sur} is the daily accumulated runoff (mm), R_{day} is the daily precipitation (mm), I_a is the initial cumulative surface storage, interception, and infiltration (mm), and S is the retention parameter (mm). The SCS curve number describes the soil's permeability in relation to LULC and prior soil water conditions (Neitsch et al. 2011). Surface storage and interception both pertain to the type of vegetation found on the LULC.

Percolation

Percolation occurs once the first soil layer reaches field capacity and the layer below is not already saturated. It is calculated using storage routing methodology as:

$$w_{per,lyr} = SW_{lyr,exc} * \left(1 - e\left[\frac{-\Delta t}{TT_{per}}\right]\right) \quad (3)$$

where $w_{per,lyr}$ denote the amount of water percolating daily to the underlying soil layer (mm), $SW_{lyr,exc}$ is the daily drainable volume of water in the soil layer (mm), Δt is the time step given in hours, and TT_{per} is the time it takes for the water to percolate in hours. The travel time is different for each soil layer and is therefore calculated independently for each layer in the dataset as:

$$TT_{per} = \frac{SAT_{lyr} - FC_{lyr}}{K_{sat}} \quad (4)$$

where SAT_{lyr} is the water content in the layer upon complete saturation (mm), FC_{lyr} is the water content in the layer at field capacity (mm), and K_{sat} is the saturated hydraulic conductivity for the layer (mm h^{-1}) (Neitsch et al. 2011).

Lateral flow is an important constituent in soils with high hydraulic conductivity at the surface layer and impermeable layer below as it transports a significant amount of water. SWAT incorporates a kinematic storage model developed by Sloan and Moore (1984) to estimate subsurface flow on hillslope segments.

Groundwater flow

A shallow and a deep aquifer is computed for each sub basin within the watershed, where shallow aquifers contribute directly to the streamflow, while deep aquifers are assumed to contribute to streamflow somewhere outside the watershed (Arnold et al. 1993). The amount of water contributing to streamflow through the shallow aquifer is defined as the groundwater flow and calculated as:

$$Q_{grw} = \frac{8000 * K_{sat}}{\left(L_{grw}\right)^2} * h_{tbl} \quad (5)$$

where Q_{grw} denotes the groundwater flow (mm day^{-1}), K_{sat} is the hydraulic conductivity of the aquifer (mm day^{-1}), L_{grw} is the distance between the sub-basin divide and the main channel (m), and h_{tbl} is the height of the water table (m).

Actual and potential evapotranspiration

Potential evapotranspiration within the SWAT-model was calculated from the Hargreaves method (Hargreaves and Samani 1985) as it requires the least ancillary parameters to function. The function used to determine the amount of potential evapotranspiration is:

$$\lambda E_o = 0.0023 * H_0 * (T_{max} - T_{min})^{0.5} * (T_{ave} + 17.8) \quad (6)$$

where λ denotes the latent heat of vaporization (MJ kg^{-1}), E_o is the potential evapotranspiration (mm day^{-1}), H_o is the extra-terrestrial radiation (MJ m^{-2} day^{-1}), T_{max} is the maximum daily air temperature (°C), T_{min} is the minimum daily air temperature (°C), and T_{ave} is the mean daily air temperature (°C).

Actual evapotranspiration is calculated from the PET by first subtracting the precipitation intercepted by the canopy to find the amount of soil evaporation that occurs (Neitsch et al. 2011). Canopy storage and the subsequent evaporation thereof is calculated as:

$$can_{day} = can_{max} * \frac{LAI}{LAI_{max}} \quad (7)$$

where can_{day} is the maximum amount of water trapped by the canopy daily (mm), can_{max} is the amount of water the canopy can hold once it is fully developed (mm), LAI is the leaf area index, and LAI_{max} is the maximum leaf area index for the plant. Any precipitation that occurs within the watershed is first routed through the canopy storage until it is full. The model will evaporate all water from the canopy unless PET is less than the amount of water stored, in which case:

$$R_{INT(f)} = R_{INT(i)} - E_{can} \quad (8)$$

where $R_{INT(f)}$ is the final amount of water stored in the canopy (mm), $R_{INT(i)}$ is the initial amount stored in the canopy (mm), and E_{can} is the amount of water evaporated from the canopy (mm). Any precipitation occurring after the canopy storage is full is transported to the next stage, where the model calculates the amount of water evaporated from the soil as:

$$E_s = E'_o * e^{(-5.0*10^{-5}*CV)} \quad (9)$$

where E_s denotes the maximum daily soil evaporation (mm), E'_o is the potential evapotranspiration after adjusting for evaporation from the canopy storage (mm), and CV is the aboveground biomass

and litter (kg ha^{-1}). The amount of water evaporated from the soil is highly dependent on shading from plants and topography (Neitsch et al. 2011).

Sediment yield

Sediment yield in the main channel is computed from the Modified Universal Soil Loss Equation (MUSLE) (Williams 1974) as an implementation within the SWAT model (Arnold et al. 2012b) as:

$$sed = 11.8 * \left(Q_{sur} * q_{peak} * area_{hru}\right)^{0.56} * K_{USLE} * C_{USLE} * P_{USLE} * LS_{USLE} * CFRG \quad (10)$$

where sed is the daily sediment yield (metric tons), Q_{sur} is the amount of surface runoff (mm ha^{-1}), q_{peak} is the peak runoff rate (m^3 s^{-1}), $area_{hru}$ is the area of the HRU (ha), K_{USLE} is the USLE soil erodibility factor (0.013 metric ton m^2 hr/(m^3-metric ton cm)), C_{USLE} is the management and cover factor, P_{USLE} is the support practice factor, LS_{USLE} is the USLE topographic factor, and $CFRG$ is the coarse fragment factor (Neitsch et al. 2011). The soil erodibility factor is estimated from the equation proposed by Williams (1974):

$$K_{USLE} = f_{csand} * f_{cl-si} * f_{orgc} * f_{hisand} \quad (11)$$

where f_{csand} is a parameter, which assigns high erodibility to soils with low coarse sand content and vice versa, f_{cl-si} is a parameter that assigns a low erodibility to soils with high clay to silt ratios, f_{orgc} is a parameter that assigns lower erodibility to soils with higher organic carbon content, and f_{hisand} is a parameter that reduces soil erodibility for soils with high sand contents (Arnold et al. 2012a). The K_{USLE} factor was not specified in the soil database and had to be calculated from the particle ratios and organic content. Support practices were not considered in the estimation of sediment yield.

LULC

The primary function of the LULC classification is to define the available canopy storage/interception (7), above-ground biomass, (potential) evapotranspiration (9), and the C_{USLE} factor. Additional variables within the LULC classification pertains to the type of vegetation, which responds to the heat units calculated from temperature to estimate the growth and potential canopy storage/interception. Table 2 describes the parameters used and estimated vegetation type for each LULC class. The growth is also dependent on available water, which is indicated by the water stress. This variable is 0.0 under optimal conditions and approaches 1.0 as areas become increasingly water

stressed. A value of 1 denotes no transpiration and 0 is when actual transpiration = potential transpiration. It is calculated by comparing the actual and potential plant transpiration on a given day:

$$wstrs = 1 - \frac{E_{t,act}}{E_t}$$

where $wstrs$ is the water stress, $E_{t,act}$ is the actual amount of transpiration (mm day^{-1}), and E_t is the maximum amount of transpiration (mm day^{-1}).

Table 2: Vegetated LULC classes from the SWAT database used to classify the study area. T_{base} is the base temperature used to estimate plant growth (°C), T_{opt} is the optimal temperature for plant growth (°C), LAI_{mx} is the maximum leaf area index, $h_{c,mx}$ is the maximum canopy height (m), $z_{root,mx}$ is the maximum rooting depth (m), and $C_{usle,mn}$ is the minimum estimated USLE C factor for each LULC type.

LULC class	Vegetation type	T_{base}	T_{opt}	LAI_{mx}	$h_{c,mx}$	$z_{root,mx}$	$C_{usle,mn}$
Cultivated	Grain Sorghum	11	30	3	2.5	2	0.2
Pasture	Bermudagrass	12	25	4	0.5	2	0.003
Grassland	Little Bluestem	12	25	2.5	1	2	0.003
Bush/shrubland	Little Bluestem	12	25	2	1	2	0.003
Forest	Oak	10	30	5	6	3.5	0.001

Urban areas

The primary difference between areas of natural vegetation or agriculture and urban areas is the imperviousness of the latter. In the SWAT model, impervious areas are differentiated into two groups: areas that are hydrologically connected to the drainage system and those that are not (Neitsch et al. 2011). The default parameters for urban areas were modified to better fit the conditions of the watershed. The urban areas were classified from the density of houses and the connecting roads within each settlement. Low- and medium/low-density settlements had no paved roads and therefore a 0% imperviousness. The medium-density settlements were distinguished from their paved roads and relatively high density of houses within each settlement. However, only approximately half the major roads were paved, and the imperviousness was therefore halved from the default setting to 20%. For the impervious hydrologically connected area, an SCS curve number of 98 was used (Neitsch et al. 2011), while disconnected impervious areas were calculated as:

$$CN_c = CN_p + imp_{tot} * \left(CN_{imp} - CN_p\right) * \left(1 - \frac{imp_{dcon}}{2 * imp_{tot}}\right) \quad (12)$$

where CN_c is the composite moisture condition II curve number, CN_p is the pervious moisture condition II curve number, CN_{imp} is the impervious moisture condition II curve number, imp_{tot} is the impervious fraction of the HRU, and imp_{dcon} is the disconnected impervious fraction of the HRU.

Results

Land use/Land cover

The classification of LULC between 1989 and 2019 shows major changes in all classes except forests and low-density settlements (table 3). However, in the cross-tabulation, only 50% of the area classified as forest in 1989 was also designated forest in 2019, while much of the original area had been converted to agriculture or bush/shrubland (table 5). The cross-tabulation shows the intersect between the different LULC classes for the two study periods. The columns describe the original LULC in 1989 and adds up to 100%. The rows show the LULC in 2019 with intersect between the original LULC and areal change. Less than 100% in classes of 2019 indicate a decrease, while values above 100% show an increase in that class. Smaller areas in 2019 were classified as forest, which in 1989 had belonged to other classes. For bush/shrubland in 1989 only 34% of the original area remained in the same class in 2019, while much of the remaining land was converted to agriculture. However, 34% of the area classified as grassland in 1989 falls under bush/shrubland in 2019. Grassland as the third constituent of the natural vegetation class lost the largest fractional area to cultivated areas but also lost a third of its total area to bush/shrubland. These increases in cultivated areas at the expense of natural vegetation results in the largest absolute growth of cultivated areas over the 30-year period (table 3). This is also apparent from table 3, which shows that just under half of natural vegetation in 1989 has been converted to cultivated areas by 2019. Pasture and bare soils both experienced large relative decreases but amounted to less than 5% of the entire watershed combined. Areas of bare soil also showed no continuity between 1989 and 2019 as most areas previously categorized as bare soils were classified as either cultivation or bush/shrubland in 2019. Similarly, pasture also did not display any continuity between the two study periods but instead showed an almost full conversion to cultivation from 1989 to 2019 (table 5).

Built-up areas show gradual increases from low-density settlements up to medium-density settlements and additionally displays the largest fractional increase overall (table 3). The changes are largely observed within the class of built-up areas, where low-density settlements have developed into medium/low-density settlements from 1989 to 2019 (table 4 & 5). A similar trend is observable in the higher density settlements with areas growing from medium/low- to medium-density settlements.

Table 3: Area of LULC classes identified in 1989 and 2019 (in hectares and percentage of total area) and the change from the first to the latter (in ha and %).

	1989		2019		Change	
LULC class	**ha**	**%**	**ha**	**%**	**ha**	**%**
Bare soil	2285	3.5	438	0.7	-1848	-81
Cultivated areas	19566	30.2	33541	51.7	13975	71
Pasture	1142	1.8	109	0.2	-1033	-90
Grassland	9553	14.7	774	1.2	-8780	-92
Bush/Shrubland	18974	29.3	12998	20.0	-5976	-31
Forest	6094	9.4	5601	8.6	-493	-8
Low-density settlement	5267	8.1	6011	9.3	744	14
Medium/low-density settlement	1737	2.7	3773	5.8	2037	117
Medium/density settlement	223	0.3	765	1.2	542	243
Cloud cover*	0	0.0	831	1.3		
Total area	64841		64841			

Table 4: Cross tabulation between the three major categories of LULC between 1989 (columns) and 2019 (rows). Areal change is listed in percentage.

	1989		
2019	**Agricultural areas**	**Natural vegetation**	**Built-up areas**
Agricultural areas	75.4	43.6	28.0
Natural vegetation	8.7	47.6	6.0
Built-up areas	14.3	8.0	63.9

Table 5: Cross tabulation between all LULC classes observed in the watershed. Change is given in percentage between 1989 (columns) and 2019 (rows).

	1989								
2019	**Bare soil**	**Cultivated area**	**Pasture**	**Grassland**	**Bush/ Shrub land**	**Forest**	**Low-density settlement**	**Medium/low-density settlement**	**Medium-density settlement**
Bare soil	0.0	1.7	1.7	0.2	0.3	0.0	0.0	0.1	0.0
Cultivated areas	18.4	73.9	95.0	52.3	46.0	29.9	32.6	16.9	5.0
Pasture	0.0	0.4	0.0	0.0	0.0	0.0	0.0	0.0	0.0
Grassland	0.0	1.3	0.0	1.6	0.8	2.5	1.2	0.0	3.3
Bush/Shrubland	77.3	3.9	1.4	33.5	34.2	9.7	3.3	0.0	0.0
Forest	2.6	2.2	0.0	1.1	9.2	50.3	2.8	1.5	6.1
Low-density settlement	0.2	8.7	0.0	6.1	6.9	2.2	34.2	27.1	0.0
Medium/low-density settlement	1.5	5.3	1.2	4.5	2.1	0.2	22.5	38.1	0.0
Medium-density settlement	0.0	1.1	0.0	0.4	0.1	0.1	0.5	16.3	85.6

The growth in agriculture has primarily occurred near built-up areas (figure 4) and on the slopes surrounding the watershed (figure 5). The expansion of settlements into areas previously uninhabited has resulted in a removal of the natural vegetation, which is visible in the south-eastern and northern region. Few places around the more populated areas have maintained their natural vegetation due to the sheer steepness, which makes cultivation unfeasible. Another natural inhibitor is the streams generated by runoff from the slopes, which creates tunnels of forests along the riverbanks and is present in both 1989 and 2019, although with a significant decrease in size in the latter year. The last major homogenous area to remain uncultivated lies near the outlet of the watershed, where bush/shrubland dominate the floodplain and forests inhabit the mountains. Several settlements have however, been built along the boundary to this area in the period between 1989 and 2019.

The development of built-up areas is also visible in figure 4, which shows the lower density settlements becoming increasingly populated. This trend is especially pronounced within the floodplain and on the plateaus, which are regions that have been populated for a long time.

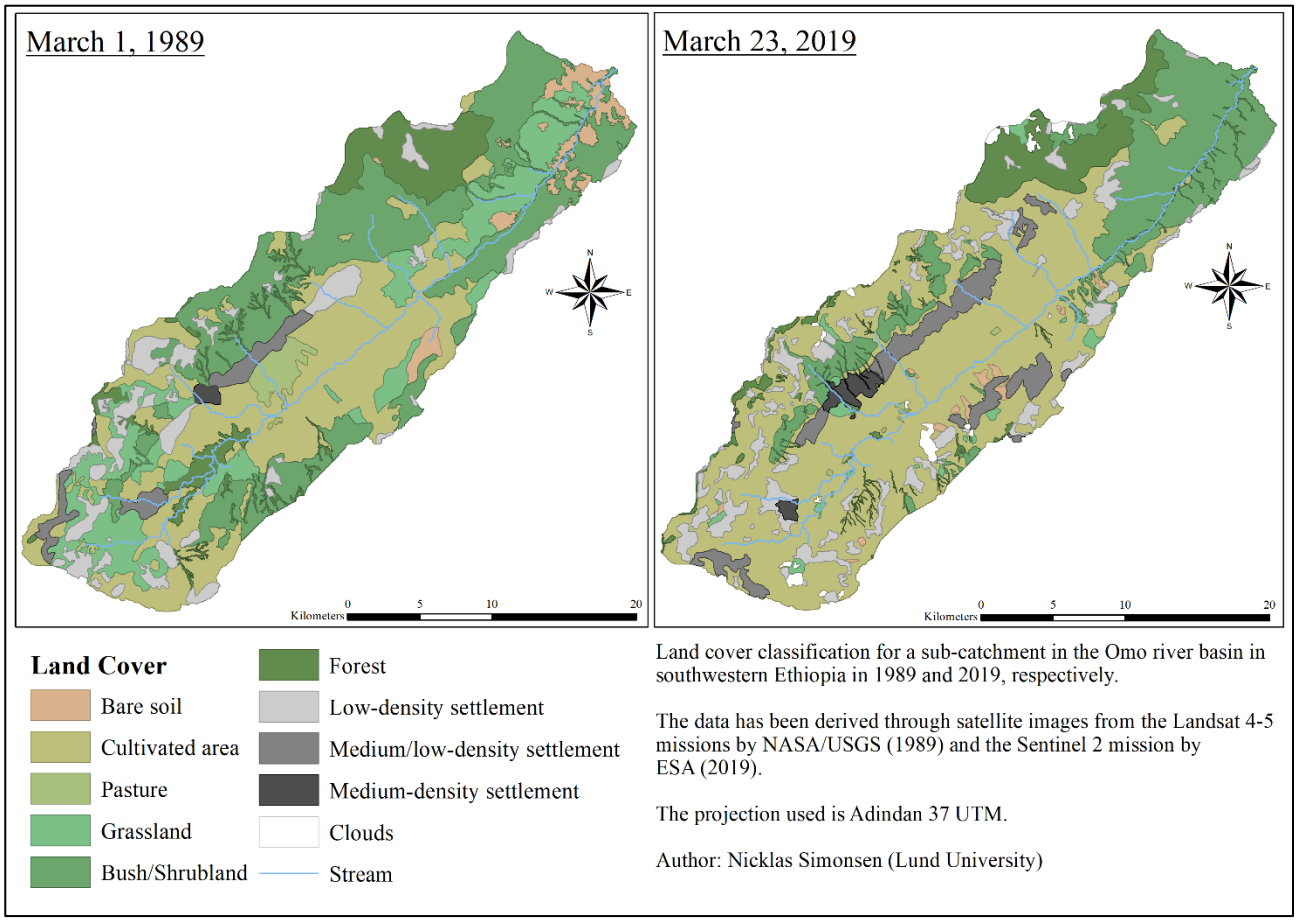

Figure 4: LULC classification of the study area in 1989 and 2019, showing the spatial change of classes.

The largest change in LULC between 1989 and 2019 can be attributed to the expansion of agriculture in the form of cultivated fields (table 3). Figure 5 shows how this change is distributed spatially across the various slopes within the watershed. The coloured background indicates contour intervals of 200m for cultivated areas. All other LULC classes are removed to represent the relative expansion of agriculture. It illustrates how the slopes have become increasingly subject to cultivation from 1989 to 2019.

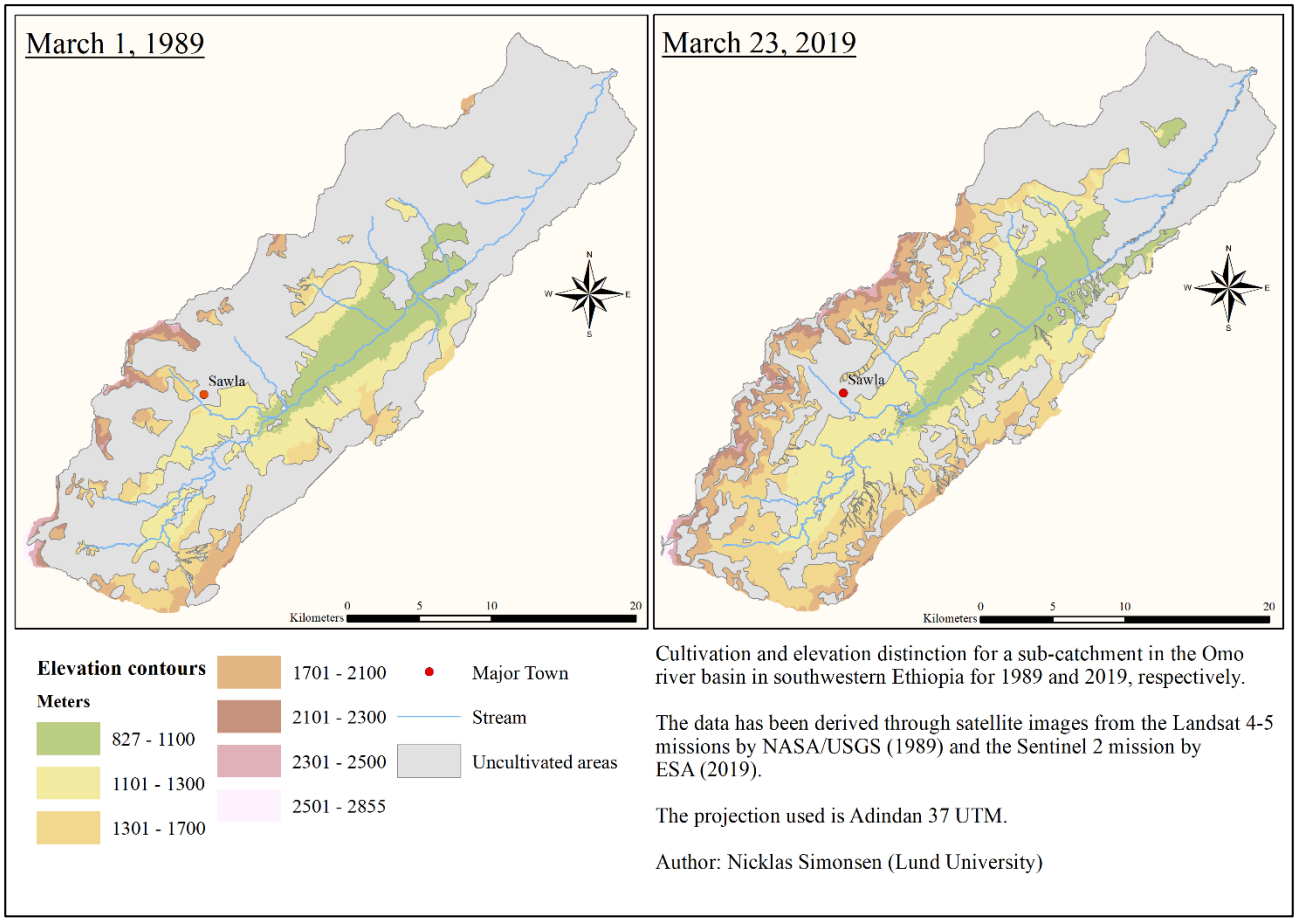

Figure 5: Distribution of cultivated areas at different elevations within the watershed between 1989 and 2019.

Classification accuracy

The confusion matrix (table 6) shows an acceptable level of error in the classification (>80%). The settlements all scored high on the accuracy assessment with values between 82-96%, while other classes such as bare soil, grasslands, and forests scored much lower. Both user's and producer's accuracy were low for grasslands (25%) but also only contained 8 points due to its relatively small area in 2019. Cultivated areas and bush/shrubland were the most common classes and both scored 86%.

Table 6: Confusion matrix of the LULC classification in 2019 against the ground truth. Areas correctly classified = 256; overall classification accuracy: 82%; class 1: Bare soil; class 2: Cultivated areas; class 3: Pasture; class 4: Grassland; class 5: Bush/shrubland; class 6: Forest; class 7: Low-density settlement; class 8: Medium/low-density settlement; class 9: Medium-density settlement.

Classified data	**1**	**2**	**3**	**4**	**5**	**6**	**7**	**8**	**9**	**Row total**	**User accuracy**
1	5	1	0	2	2	0	0	0	0	10	50%
2	3	125	0	1	11	3	2	0	1	146	86%
3	0	2	9	0	0	0	0	0	0	11	82%
4	0	1	0	2	1	4	0	0	0	8	25%
5	2	3	0	1	50	1	1	0	0	58	86%
6	0	3	0	2	3	16	0	0	0	24	67%
7	0	0	0	0	0	0	26	1	0	27	96%
8	0	2	0	0	0	0	1	14	0	17	82%
9	0	0	0	0	0	0	0	1	9	10	90%
Column total	10	137	9	8	67	24	30	16	10	311	
Producer's accuracy	50%	91%	100%	25%	75%	67%	87%	88%	90%		Kappa index: 0.76

Climate

The rate and quantity of precipitation over the study area has experienced regular decadal oscillations but has from 2010 to 2013 been more extreme than previous highs (figure 6). The maximum daily precipitation has followed the same trend within the same period (1989-2013).

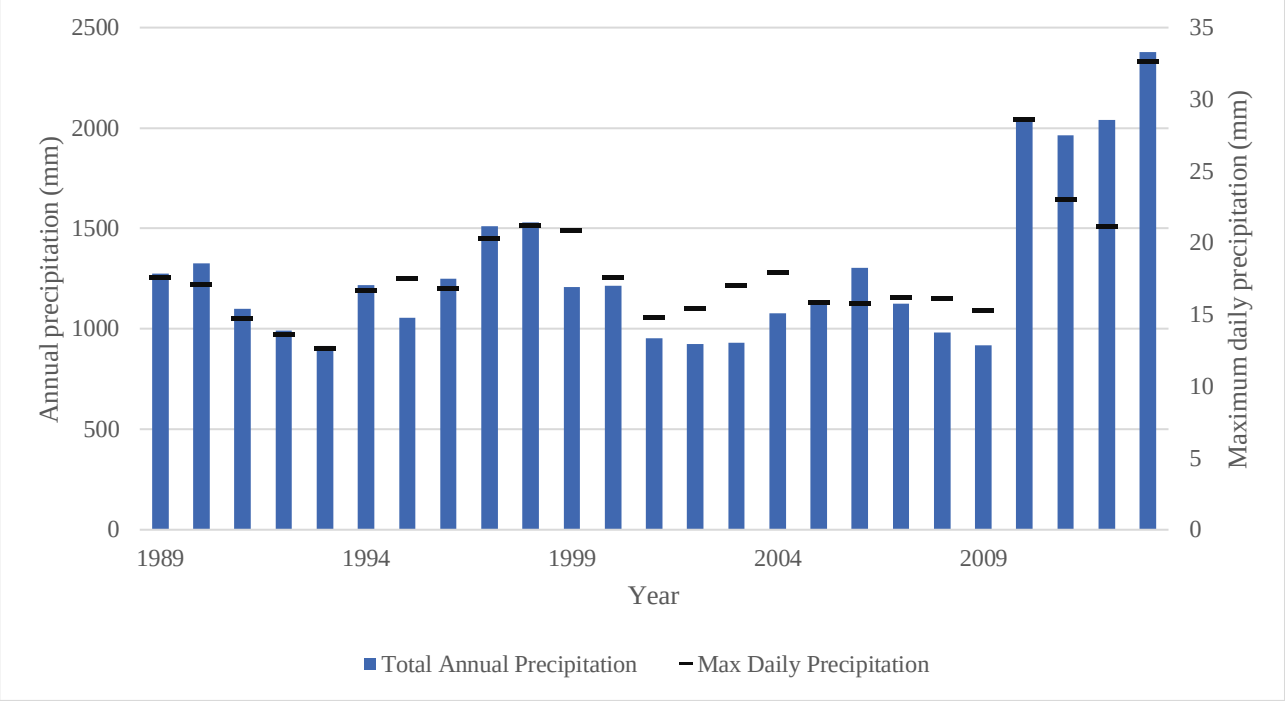

Figure 6: Total annual and maximum daily precipitation from 1989-2013 over the watershed using CFSR data.

The monthly variation in precipitation over the watershed is visible in figure 7, which shows the beginning of the wet season and the annual maximum for precipitation in April and a secondary lesser peak in in October. Daily maximum precipitation is displayed for the two study periods and the two projections. It shows only a slight increase from 1989 to 2079 in the first wet season but a much more pronounced increase during the second wet season in October.

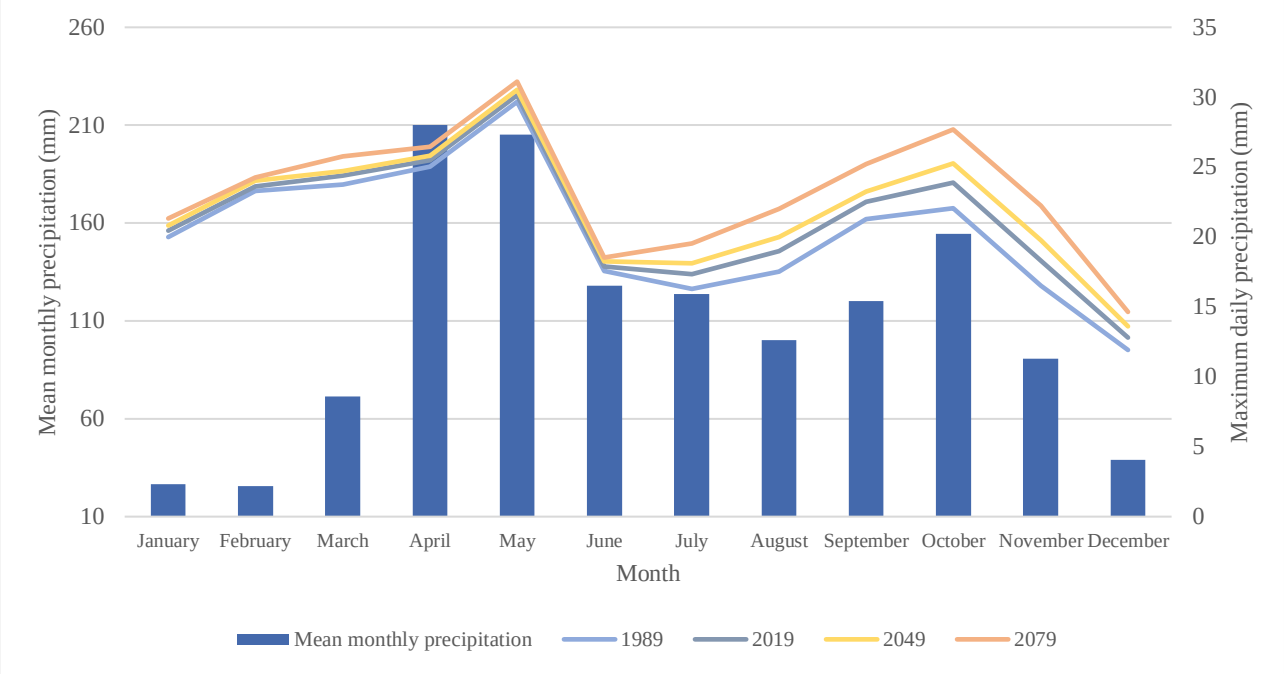

Figure 7: Mean monthly precipitation (1989-2013) and measured maximum daily precipitation for 1989 (blue) and 2019 (grey). Projected maximum daily precipitation is shown for 2049 (yellow) and 2079 (orange).

Temperatures in the watershed did not vary significantly between 1989 and 2019 but a much higher interannual fluctuation in maximum temperatures were observed than minimum (figure 8). Additionally, while minimum temperatures within the study area gradually increased in all months from 1989 to 2079, maximum temperatures had a much larger increase towards the end of the century. This change is homogenous across all months with no distinct variation between months.

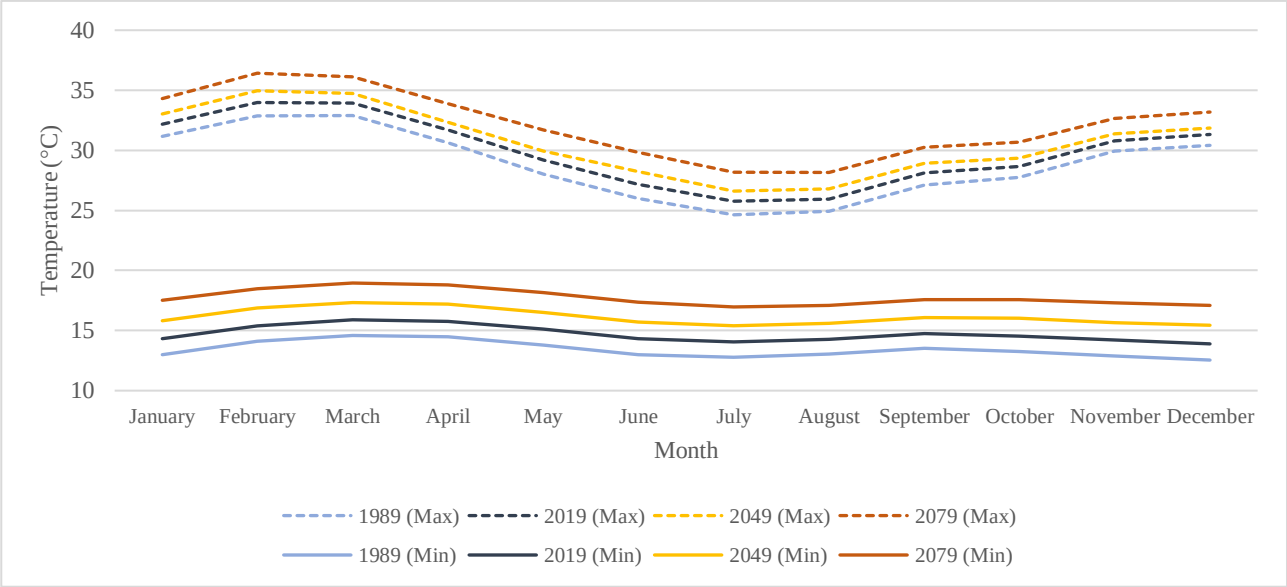

Figure 8: Mean maximum and minimum monthly temperatures in 1989 (blue) and 2019 (grey). Projected values are shown for 2049 (yellow) and 2079 (orange).

Watershed hydrology

The estimated amount of monthly precipitation and sediment yield for the four modelling periods are shown in figure 9 and 10. Precipitation estimations are the product of interpolation between the CFSR grid cell centroids. The projections show an overall increase in precipitation with time but also a distinct enhancement of the secondary wet season in October. For February, June, and September, 1989 shows the highest cumulative precipitation but for most other months it increases towards the end of the 21st century.

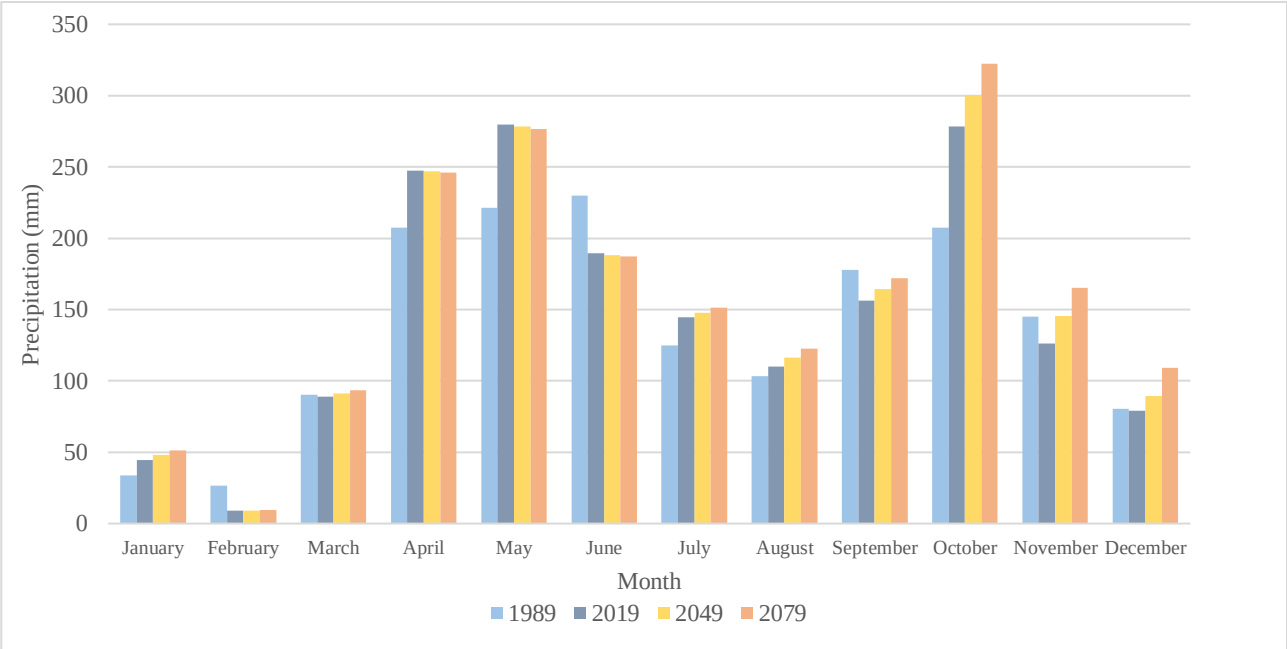

Figure 9: Total monthly precipitation measured in 1989 (blue) and 2019 (grey) and projections for 2049 (yellow) and 2079 (orange).

The results from the model show a significant continuous increase in precipitation at approximately 5% per 30 years or between each modelled interval (table 7). This also results in changes in flows with significant increases in runoff for 2019 and onwards. Lateral flow is the only negative trend in the modelled hydrological cycle but only decreases initially between 1989 and 2019, after which it continues to increase with time. Groundwater flow; evapotranspiration; and potential evapotranspiration all show continuous increase with time. Sediment yield increases drastically from 1989 to 2019 but experiences a slight decrease in 2049, after which it increases again gradually.

Table 7: The hydrological components computed from the SWAT, showing the relative change from values in 1989. All values are given in percent change from the 1989 values. R is precipitation, Q_{sur} is surface runoff, Q_{lat} is lateral flow, Q_{grw} is groundwater flow, E_a is evapotranspiration, E_o is potential evapotranspiration and sed is sediment yield.

	R (%)	Q_{sur} (%)	Q_{lat} (%)	Q_{grw} (%)	E_a (%)	E_o (%)	sed (%)
2019	6.4	33.1	-7.3	12.9	5.2	7.4	129.4
2049	10.8	38.3	-3.1	19.9	8.8	11.5	128.6
2079	15.7	44.3	1.5	22.3	13.6	16.7	134.7

The results for the monthly sediment yield in all four years show a large increase in the wet season from the estimated yield in 1989 (figure 10). However, the total monthly yield appears to decrease during the initial wet season of April, May, and June for years beyond 2019, while the second wet season in October and November shows a sharp increase for the same years. A similar trend is observable in the precipitation estimates for the two wet seasons (figure 9).

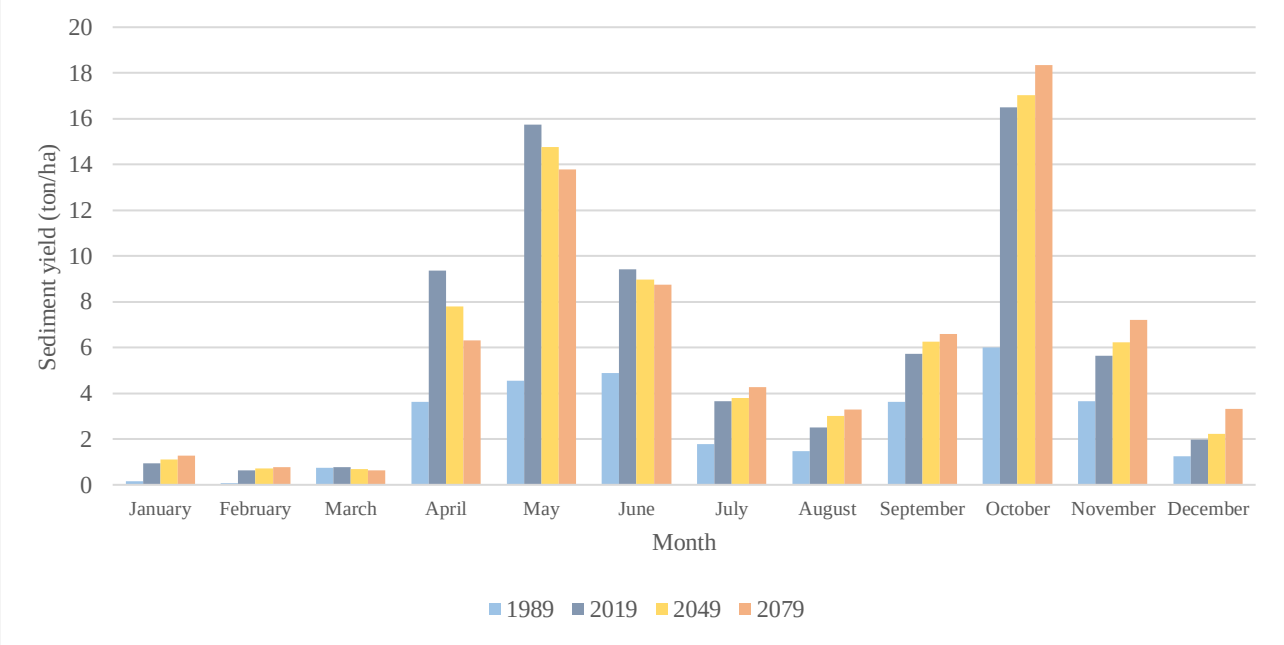

Figure 10: Total monthly sediment yield for 1989 (blue), 2019 (grey), 2049 (yellow), and 2079 (orange).

Discussion

The results from the model support the empirical evidence of land degradation from anthropogenic LULC change observed and modelled by others (Hurni 1988, 1993; Nyssen et al. 2004; Gessesse et al. 2015; Sewnet and Abebe 2018; Bekele et al. 2019a). It shows that a conversion of natural vegetation to cultivation or settlements has led to a significant increase in runoff and sediment yield in the Sawla watershed. Although this increase occurred in conjunction with changes in the climate, it cannot be explained solely from these changes. Variations in precipitation and temperature did have some effect on runoff and sediment yield but the incremental change between the years of changing climate (2019 to 2049/2079) are far less than those of LULC and climate change combined (1989 to 2019). These findings agree with other studies (Lemann et al. 2018; Bekele et al. 2019a) from different parts of Ethiopia and indicate a socioeconomic pressure far greater than that of a changing climate. Studies (Lambin et al. 2001; Nyssen et al. 2004; Bekele et al. 2019a) suggest that the conversion of natural vegetation to agriculture is a result of population pressure and limited economic opportunities.

The projections for 2049 and 2079 do not consider continuous changes in LULC as observed between 1989 and 2019. Although some change is likely to occur, the rate will significantly decrease due to the amount of land available for conversion. In 1989 natural vegetation constituted more than half of the total LULC of the watershed, while in 2019 it made up under a third. Additionally, many of the areas still vegetated by forests or shrubs/bush in 2019 are in areas inaccessible to humans or unfeasible for cultivation.

Ethiopia has since 1995 (Nyssen et al. 2004) been implementing soil and water conservation (SWC) structures such as stone bunds and terracing to reduce the amount of runoff and erosion. Betrie et al. (2011) found that the implementation of stone bunds reduced sediment yields by 9-69%, but that efficiency decreased with slope and larger areas of agriculture. Gebremichael et al. (2005) showed a similar efficiency of stone bunds at 68% reduction but also pointed out that the storage capacity of the bunds is finite and requires regular maintenance to effectively reduce erosion. Due to the lack of field data and the coarse resolution of the Landsat imagery, these structures have not been included in the assessment of LULC in this study. It is likely that the runoff and sediment yield has been overestimated in 1989 and forwards due to this limitation. This may have a bigger influence on the LULC in 2019 due to increased cultivation on slopes, and the drastic increase in runoff and sediment yield from 1989 could be overestimated. However, the SWC reduction measurements are site-based and may not apply homogenously throughout the watershed. Hence, extensive field data

would be required to properly estimate any watershed practicing SWC. Addis et al. (2016) showed that the SWC were only effective during periods of low precipitation and did not affect the runoff rates significantly during periods of intense precipitation. This is an important aspect to consider as the intensity of precipitation events over the watershed are projected to increase in the future.

Sediment yield results from other studies in Ethiopia vary between 1 and >150 t ha^{-1} yr^{-1} (Betrie et al. 2011; Michael Mamo and K. Jain 2013; Gessesse et al. 2015; Addis et al. 2016) with an average observed yield of 42 t ha^{-1} yr^{-1} (Gebremichael et al. 2005). This indicates a high spatial variability and dependence on local environmental conditions. Hence, it may be difficult to verify findings of one study based on the results from another. Despite these limitations, the results from this study shows yields of 32 and 73 t ha^{-1} yr^{-1} for 1989 and 2019, respectively. While these estimates cannot be verified, they still indicate a strong positive trend in yields caused by the conversion of natural vegetation to agriculture.

The discrepancy between the cumulative runoff and sediment yield for 2019 and onwards is likely caused by separate rates of expansion from cultivation and settlements. Cultivated land tends to increase sediment yield (Hurni 1988; Moges and Holden 2009; Alemneh et al. 2019), while settlements decrease permeability and thus contribute to greater runoff (Bronstert et al. 2002). Cultivated areas grew by 20% of the total watershed area from 1989 to 2019, while settlements expanded by 5% of the total watershed and mostly in low and low/medium density settlements. As the LULC continues to evolve past 2019 and suitable areas for cultivation diminish, it is likely that settlements will at some point expand faster than agriculture as the population grows. This change has been predicted for other watersheds in Ethiopia (Gashaw et al. 2018; Kidane et al. 2019) and will lead to a shift in the hydrology dynamics of the watershed. Other studies found that the conversion of natural vegetation to cultivation led to changes in the discharge regime. Increased cultivation resulted in lower baseflow during the dry season and increased streamflow during the wet season (Gebremicael et al. 2019; Kidane et al. 2019), thus aggravating the risk of floods (Permatasari et al. 2019).

The pronounced unimodal wet season may develop into a bimodal under current projections. The secondary lesser wet season in October is set to become the more pronounced of the two as precipitation increases towards the end of the century. The intensity of precipitation events is projected to increase in the second semester with little to no change in the first half of the year. This development is coupled with a decrease in precipitation of the primary wet season from 2019 and onwards. Both minimum and maximum temperature is predicted to increase for all projected periods.

Minimum temperature for all months increases faster than maximum temperature, which agrees with findings by other studies (Bekele et al. 2019b). These local temperature trends are predicted (Dessu and Melesse 2012) to have less effect on the watershed hydrology than the large-scale temperature increments over the Indian Ocean, which will result in more precipitation over East Africa.

An unexpected result was the increase in evapotranspiration despite having less vegetation in 2019. Gashaw et al. (2018) found conflicting results from the LULC in Ethiopia with a general decrease in ET as natural vegetation declines in favour of cultivated land. The increase in ET for the study area likely stems from higher temperatures and more precipitation in the climate scenarios, while the LULC seems to have little to no effect on it. The amount of water stress days for all simulated study periods was 11.4±0.5 and showed no discernable pattern between the years. The temperature stress days however, decreased steadily from 19.5 in 1989 to 2.6 in 2079, which is due to the higher optimal temperature of the agricultural biomass than the bush/shrublands and grasslands.

The LULC the watershed sustained between 1989 and 2019 had a higher overall impact on the watershed hydrology than the temperature and precipitation increments. Components such as sediment yield and runoff were especially affected by the changes in land cover/use, while the subsurface fluxes like lateral- and groundwater flow showed higher dependence on climactic factors. These parameters are of course not independent as increases in surface runoff is often at the expense of a decrease in subsurface flows, while ET depends on both land cover/use and climate factors. Hence, it is important to consider the development of the watershed hydrology as a single unit rather than two separate ones. To further understand the balance of the watershed in future projections, dynamic LULC models would have to be implemented. This is beyond the scope of this paper but may be of interest to other studies wishing to thoroughly examine watershed hydrology under climate change.

Limitations

The use of CFSR data in lieu of ground observations from meteorological stations can be advantageous due to its complete record and full coverage. Studies (Dile and Srinivasan 2014; Worqlul et al. 2014; Tolera et al. 2018) show that the CFSR data performs well for streamflow and precipitation estimations compared to ground data in larger watersheds, but fail to capture the climactic conditions of smaller watersheds (Roth and Lemann 2016). The lack of access to ground data in the Sawla watershed may have led to inputs that were not fully representative of the hydrological conditions. The projections for 2049 and 2079 were based on the same CFSR dataset

and thus face the same limitations. In addition, future estimates from models were generalized for the entirety of Ethiopia and hence does not reflect the local conditions of the watershed.

The lack of ground truth also applies to the land cover interpretation, which used generic classes specified by the SWAT database. This means that certain assumptions based on the spectral and geometric signature had to be made. Pasture and grassland are nearly identical when observed from satellite imagery but possess widely different hydrological characteristics. Low grasses could also not be distinguished from bare soil and thus some of the land cover dependent parameters may not be representative of the actual conditions.

Additional limitations were imposed on the future projections by assuming an unchanged LULC from 2019 and onwards. This is not likely to be true in a real-world scenario but due to the scope of this study, a LULC model was not implemented. It is therefore likely that some variables were underestimated, if considering the trend from 1989-2019. However, the amount of land eligible for conversion to anthropogenic purposes is finite and will likely not continue at the same rate as between 1989-2019.

The climate of the watershed was calculated with a daily time-step using average monthly values; standard deviation; and skew within each month. This resulted in relatively smooth weather during the simulations, which may not be representative of actual conditions. This may be an important factor to consider when interpreting the runoff/sediment yield numbers, as more extreme weather events will spike these numbers. This limitation is perhaps more important for future projections, as it does not consider an increase in extreme events resulting from climate change.

The difference in resolution between the Landsat 4-5 TM and Sentinel 2 satellite imagery may have led to different interpretations of the land cover. At 30-meter resolution, many smaller objects such as individual houses and settlements go undetected. This may have resulted in an underrepresentation of small low-density settlements.

Hydrological data is scarce in Ethiopia and only relatively few river basins are measured with stream gauges. This makes calibration and verification of models such as SWAT impossible outside of the select few river basins. This study attempted to work around that limitation by providing incremental differences between modelling periods rather than absolute numbers. This was to examine the impacts of LULC and climate on the hydrological dynamics within the watershed to estimate the scope of change. However, results should be interpreted from the notion that they are

merely an indication of the direction and rate of change rather than a direct assessment of the hydrology.

Conclusion

This study can conclude that anthropogenic LULC such as increased agriculture and settlements has led to significantly larger rates of runoff and sediment yield. More precipitation and higher temperatures as a result of climate change has also led to an intensification of the hydrological cycle within the watershed but not at the same magnitude as LULC. The Sawla watershed experienced a 58% increase in cultivation at the expense of natural vegetation from 1989 to 2019. This resulted in a 33% and 129% increase of the runoff and sediment yield, respectively. This steep increase was caused by a growing number of cultivated areas on steep slopes, which replaced otherwise natural vegetation such as forest and bush/shrubland. The increased agriculture is associated with more sediment yield, while the expansion of built-up areas can be attributed to higher runoff rates. Although the watershed saw a reduction in natural vegetation, ET continued to increase with time. Other studies found contradictory results, but this may reflect on the high heterogeneity between watersheds.

Other constituents of the hydrological cycle were less affected by the LULC but responded to changes in climate, which projected both hotter and wetter conditions in the future. Additionally, an increasingly pronounced secondary wet season was observed towards the end of the century with more precipitation and at higher intensities. The recorded and projected temperatures showed larger increases for minimum temperatures than maximum in all months.

These findings agree with those from other studies in Ethiopia and underscore the issues regarding LULC change in the developing world. Without proper mitigation from soil and water conservation interventions, these areas face degradation at alarming rates. The lack of data in these regions makes it difficult to quantify the problems and target the areas at risk, hence efforts should be made to implement more/better hydrological and meteorological coverage.

References

Addis, H. K., S. Strohmeier, F. Ziadat, N. D. Melaku, and A. Klik. 2016. Modeling streamflow and sediment using SWAT in Ethiopian Highlands. *International Journal of Agricultural and Biological Engineering,* 9**:** 51-66. DOI: 10.3965/j.ijabe.20160905.2483

Adimassu, Z., G. Alemu, and L. Tamene. 2019. Effects of tillage and crop residue management on runoff, soil loss and crop yield in the Humid Highlands of Ethiopia. *Agricultural Systems,* 168**:** 11-18. DOI: 10.1016/j.agsy.2018.10.007

Alemneh, T., B. F. Zaitchik, B. Simane, and A. Ambelu. 2019. Changing Patterns of Tree Cover in a Tropical Highland Region and Implications for Food, Energy, and Water Resources. *Frontiers in Environmental Science,* 7**:** 1-11. DOI: 10.3389/fenvs.2019.00001

Arnold, J. G., P. M. Allen, and G. Bernhardt. 1993. A comprehensive surface-groundwater flow model. *Journal of Hydrology***:** 47-69.

Arnold, J. G., J. R. Kiniry, R. Srinivasan, J. R. Williams, E. B. Haney, and S. L. Neitsch, 2012a. Soil & Water Assessment Tool Input/Output Documentation. Texas Water Resources Institute, Report TR-439, Forney, Texas, United States, 650 pp.

Arnold, J. G., D. N. Moriasi, P. W. Gassman, K. C. Abbaspour, M. J. White, R. Srinivasan, C. Santhi, R. D. Harmel, et al. 2012b. SWAT: Model Use, Calibration, and Validation. *American Society of Agricultural and Biological Engineers,* 55**:** 1491-1508.

Bekele, D., T. Alamirew, A. Kebede, G. Zeleke, and A. M. Melesse. 2019a. Land use and land cover dynamics in the Keleta watershed, Awash River basin, Ethiopia. *Environmental Hazards,* 18**:** 246-265. DOI: 10.1080/17477891.2018.1561407

Bekele, D., T. Alamirew, A. Kebede, G. Zeleke, and A. M. Melesse. 2019b. Modeling Climate Change Impact on the Hydrology of Keleta Watershed in the Awash River Basin, Ethiopia. *Environmental Modeling & Assessment,* 24**:** 95-107. DOI: 10.1007/s10666-018-9619-1

Betrie, G. D., Y. A. Mohamed, A. Van Griensven, and R. Srinivasan. 2011. Sediment management modelling in the Blue Nile Basin using SWAT model. *Hydrology and Earth System Sciences,* 15**:** 807-818. DOI: 10.5194/hess-15-807-2011

Bronstert, A., D. Niehoff, and G. Burger. 2002. Effects of climate and land-use change on storm runoff generation: present knowledge and modelling capabilities. *Hydrological Processes,* 16**:** 509-529. DOI: 10.1002/hyp.326

Central Statistical Agency, 2007. Statistical Reports of the Census for Southern Nations, Nationalities and Peoples' Region Government of Ethiopia, Report 1084 pp.

Central Statistical Authority, 1996. The 1994 Population and Housing Census of Ethiopia - Results for Southern Nations, Nationalities and Peoples' Region., Federal Democratic Republic of Ethiopia, Report 980 pp.

Copernicus Sentinel data. 2019. Sentinel 2 image data. ed. European Space Agency. Retrieved from EarthExplorer.

Dessu, S. B., and A. M. Melesse. 2012. Impact and uncertainties of climate change on the hydrology of the Mara River basin, Kenya/Tanzania. *Hydrological Processes,* 27**:** 2973-2986. DOI: 10.1002/hyp.9434

Dile, Y. T., and R. Srinivasan. 2014. Evaluation of CFSR climate data for hydrologic prediction in data-scarce watersheds: an application in the Blue Nile River Basin. *Journal of the American Water Resources Association,* 50**:** 1226-1241. DOI: 10.1111/jawr.12182

FAO/IIASA/ISRIC/ISS-CAS/JRC. 2012. Harmonized World Soil Database (version 1.2). 1-50. Rome, Italy and Laxenburg, Austria: FAO and IIASA.

Gashaw, T., T. Tulu, M. Argaw, and A. W. Worqlul. 2018. Modeling the hydrological impacts of land use/land cover changes in the Andassa watershed, Blue Nile Basin, Ethiopia. *Science of The Total Environment,* 619-620**:** 1394-1408. DOI: 10.1016/j.scitotenv.2017.11.191

Gebremicael, T. G., Y. A. Mohamed, and P. Van der Zaag. 2019. Attributing the hydrological impact of different land use types and their long-term dynamics through combining parsimonious hydrological modelling, alteration analysis and PLSR analysis. *Science of the Total Environment,* 660**:** 1155-1167. DOI: 10.1016/j.scitotenv.2019.01.085

Gebremichael, D., J. Nyssen, J. Poesen, J. Deckers, M. Haile, G. Govers, and J. Moeyersons. 2005. Effectiveness of stone bunds in controlling soil erosion on cropland in the Tigray Highlands, northern Ethiopia. *Soil Use and Management,* 21**:** 287-297. DOI: 10.1111/j.1475-2743.2005.tb00401.x

Gessesse, B., W. Bewket, and A. Brauning. 2015. Model-Based Characterization and Monitoring of Runoff and Soil Erosion in Response to Land Use/land Cover Changes in the Modjo Watershed, Ethiopia. *Land Degradation & Development,* 26**:** 711-724. DOI: 10.1002/ldr.2276

Google. 2018. Google Earth image data. Mountainview, California, United States: Google.

Hargreaves, G. H., and Z. Samani. 1985. Reference Crop Evapotranspiration From Temperature. *American Society of Agricultural Engineers,* 1**:** 1-12. DOI: 10.13031/2013.26773

Hurni, H. 1988. Degradation and Conservation of the Resources in the Ethiopian Highlands. *Mountain Research and Development,* 8**:** 123-130. DOI: 10.2307/3673438

Hurni, H. 1993. Land degradation, famine, and land resource scenarios in Ethiopia. *World Soil Erosion and Conservation***:** 27-61.

Kidane, M., T. Tolessa, A. Bezie, N. Kessete, and M. Endrias. 2019. Evaluating the impacts of climate and land use/land cover (LU/LC) dynamics on the Hydrological Responses of the Upper Blue Nile in the Central Highlands of Ethiopia. *Spatial Information Research,* 27**:** 151-167. DOI: 10.1007/s41324-018-0222-y

Lambin, E. F., B. L. Turner, H. J. Geist, S. B. Agbola, A. Angelsen, J. W. Bruce, O. T. Coomes, R. Dirzo, et al. 2001. The causes of land-use and land-cover change: moving beyond the myths. *Global Environmental Change,* 11**:** 261-269. DOI: https://doi.org/10.1016/S0959-3780(01)00007-3

Lemann, T., V. Roth, G. Zeleke, A. Subhatu, T. Kassawmar, and H. Hurni. 2018. Spatial and Temporal Variability in Hydrological Responses of the Upper Blue Nile basin, Ethiopia. *Water,* 11**:** 1-35. DOI: 10.3390/w11010021

Mekonnen, M. A., A. Wörman, B. Dargahi, and A. Gebeyehu. 2009. Hydrological Modelling of Ethiopian Catchments Using Limited Data. *Hydrological Processes,* 23**:** 3401-3408. DOI: 10.1002/hyp.7470

Michael Mamo, K. H., and M. K. Jain. 2013. Runoff and Sediment Modeling Using SWAT in Gumera Catchment, Ethiopia. *Open Journal of Modern Hydrology*, 03**:** 196-205. DOI: 10.4236/ojmh.2013.34024

Moges, A., and N. M. Holden. 2009. Land Cover Change and Gully Development Between 1965 and 2000 in Umbulo Catchment, Ethiopia. *Mountain Research and Development*, 29**:** 265-276. DOI: 10.1659/mrd.00015

Neitsch, S. L., J. G. Arnold, J. R. Kiniry, and J. R. Williams, 2011. Soil and Water Assessment Tool Theoretical Documentation Texas A&M University System, Report TR-406, Temple, Texas, United States, 647 pp.

Nyssen, J., J. Poesen, J. Moeyersons, J. Deckers, M. Haile, and A. Lang. 2004. Human impact on the environment in the Ethiopian and Eritrean highlands—a state of the art. *Earth Science Reviews*, 64**:** 273-320. DOI: 10.1016/s0012-8252(03)00078-3

Permatasari, R., A. Sabar, D. K. Natakusumah, and H. Samaulah. 2019. Effects of watershed topography and land use on baseflow hydrology in upstream Komerang South Sumatra, Indonesia. *International Journal of Geomate*, 17**:** 28-33. DOI: 10.21660/2019.59.4695

Roth, V., and T. Lemann. 2016. Comparing CFSR and conventional weather data for discharge and soil loss modelling with SWAT in small catchments in the Ethiopian Highlands. 20**:** 921-934. DOI: 10.5194/hess-20-921-2016

Sajikumar, N., and R. S. Remya. 2015. Impact of land cover and land use change on runoff characteristics. *Journal of Environmental Managment*, 161**:** 460-468. DOI: 10.1016/j.jenvman.2014.12.041

Setegn, S., R. Srinivasan, and B. Dargahi. 2008. Hydrological modelling in the Lake Tana Basin, Ethiopia Using SWAT Model. *The Open Hydrology Journal*, 2**:** 49-62. DOI: 10.2174/1874378100802010049

Sewnet, A., and G. Abebe. 2018. Land use and land cover change and implication to watershed degradation by using GIS and remote sensing in the Koga watershed, North Western Ethiopia. *Earth Sci Inform***:** 99-108. DOI: 10.1007/s12145-017-0323-5

Sloan, P. G., and I. D. Moore. 1984. Modeling Subsurface Stormflow on Steeply Sloping Forested Watersheds. *Water Resources Research*, 20**:** 1815-1822.

Strauch, M., R. Otto, and M. Volk. 2015. HRU aggregation and its effects on model output. In *International SWAT Conference*, 28. Sardinia: Helmholtz.

The World Bank. 2017. World Bank Data: Ethiopia. Retrieved 06/03/2019 2019, from https://data.worldbank.org/indicator/SP.POP.TOTL?locations=ET.

The World Bank. 2019. Climate Change Knowledge Portal. Retrieved 30/04/2019 2019, from https://climateknowledgeportal.worldbank.org/country/ethiopia/climate-data-projections.

Tolera, M., I.-M. Chung, and S. Chang. 2018. Evaluation of the Climate Forecast System Reanalysis Weather Data for Watershed Modeling in Upper Awash Basin, Ethiopia. *Water*, 10**:** 1-17. DOI: 10.3390/w10060725

USGS. 1989. Landsat 4-5 Thematic Mapper imagery data. ed. U. S. G. Survey. Retrieved from EarthExplorer.

USGS. 2011. ASTER image data. ed. NASA/METI/AIST/Japan Spacesystems and U.S./Japan ASTER Science Team. Retrieved from EarthExplorer.

Van Griensven, A., P. Ndomba, S. Yalew, and F. Kilonzo. 2012. Critical review of SWAT applications in the upper Nile basin countries. *Hydrology and Earth System Sciences*, 16**:** 3371-3381. DOI: 10.5194/hess-16-3371-2012

Williams, J. R. 1974. Sediment Yield Prediction With Universal Equation Using Runoff Energy Factor. *Present and Prospective Technology for Predicting Sediment Yield and Sources***:** 17-18.

Worqlul, A. W., B. Maathuis, A. A. Adem, S. S. Demissie, S. Langan, and T. S. Steenhuis. 2014. Comparison of rainfall estimations by TRMM 3B42, MPEG and CFSR with ground-observed data for the Lake Tana basin in Ethiopia. *Hydrology and Earth System Sciences*, 18**:** 4871-4881. DOI: 10.5194/hess-18-4871-2014

Appendix A

Table A1: Soil parameters used in the SWAT model. MUID is the ID used to classify the soil, NLAYERS is the number of layers in the soil profile, and SU is the type of soil where, LPq is Lithic Leptosols, NTu is Humic Nitisols, ALu is Humic Alisols, FLe is Fluvisols, and LPd is Dystric Leptosols. SOL_Z is the depth from the soil surface to the bottom of the layer, SOL_AWC is the available water capacity of the soil layer, SOL_BD is the soil bulk densitySOL_CB is the organic carbon content (% of soil weight), CLAY is the clay content (% of soil weight), SILT is the silt content (% of soil weight), SAND is the sand content (% of soil weight), ROCK is the rock fragment content (% of soil weight).

MUID	NLAYERS	SU	SOL_Z	SOL_AWC	SOL_BD	SOL_CBN	CLAY	SILT	SAND	ROCK
ET1064	1	LPq	100	0.015	1.31	0.39	28	29	43	32
ET1210	1	NTu	1000	0.15	1.18	2.45	49	27	24	1
ET878	1	ALu	1000	0.15	1.19	2.28	32	29	39	1
ET983	1	FLe	1000	0.15	1.33	0.73	23	33	44	1
ET995	1	LPd	300	0.05	1.45	0.75	21	26	53	31

Table A2: Soil parameters calculated from existing variables or estimated from the existing SWAT database using similar soils. MUID is the ID used to classify the soil, USLE_K is the calculated USLE soil erodibility (K) factor, SOL_K is the estimated saturated hydraulic conductivity using the SWAT soil database, and SOL_ALB is the estimated soil surface albedo using the SWAT soil database.

MUID	USLE_K	*SOL_K*	*SOL_ALB*
ET1064	0.16	*186*	*0.049*
ET1210	0.15	*186*	*0.049*
ET878	0.16	*186*	*0.049*
ET983	0.17	*186*	*0.049*
ET995	0.17	*186*	*0.049*

Table A3: Climate parameters included in the SWAT model. The table lists the 25-year mean (1989-2013) variables for all stations but the model input reads each station separately, thus the table is an indication of the parameters used rather than the values. MAX_TMP and MIN_TMP is the maximum and minimum daily temperature recorded within each month, respectively, MAX_STD and MIN_STD describe the standard deviation of the temperature, PCP is the total monthly precipitation, PCP_STD is the standard deviation of the total monthly precipitation, and PCP_SKEW is the skewness of the total monthly precipitation.

25-Year Mean	MAX_TMP	MAX_STD	MIN_TMP	MIN_STD	PCP	PCP_STD	PCP_SKW
January	31.26	2.51	13.81	1.73	26.58	1.67	3.39
February	32.98	2.65	14.88	1.66	25.75	1.82	3.18
March	32.87	3.00	15.37	1.41	71.24	3.74	3.01
April	30.47	3.08	15.23	1.11	210.07	7.64	2.30
May	27.99	2.59	14.55	1.11	205.07	6.69	1.85
June	26.24	2.38	13.79	1.21	128.08	4.82	2.15
July	24.72	2.59	13.53	1.27	123.76	4.97	2.44
August	24.89	2.41	13.75	1.26	100.23	4.35	2.55
September	27.10	2.21	14.19	1.20	120.07	4.51	2.20
October	27.90	2.25	14.00	1.04	154.62	4.69	1.82
November	30.07	2.25	13.71	1.28	90.83	3.88	2.42
December	30.54	1.97	13.35	1.45	38.89	2.10	3.25

Table A4: This is a continuation of the climate parameters used in the SWAT model from table 9. PR_W1 is the probability of a wet day following a dry day, PR_W2 is the probably of a wet day following a wet day, PCPD is the average number of day of precipitation in a month, WIND is the average daily windspeed, RH is the average daily relative humidity, SOLAR is the average daily solar radiation, and RAINHHX is the maximum 0.5 hour rainfall for the month.

25-Year Mean	PR_W1	PR_W2	PCPD	WIND	RH	SOLAR	RAINHHX
January	0.18	0.56	10.24	1.57	0.46	20.76	7.40
February	0.21	0.59	10.04	1.64	0.41	21.96	7.76
March	0.37	0.70	17.91	1.65	0.50	21.43	16.72
April	0.47	0.92	26.57	1.69	0.69	21.66	33.70
May	0.36	0.96	29.06	1.72	0.77	21.64	28.73
June	0.53	0.91	26.62	1.67	0.75	18.83	20.59
July	0.50	0.91	27.82	1.55	0.75	16.39	21.93
August	0.52	0.91	27.25	1.58	0.73	17.83	19.16
September	0.57	0.90	25.93	1.59	0.70	20.21	19.11
October	0.46	0.92	26.78	1.65	0.72	21.76	19.67
November	0.28	0.81	18.21	1.61	0.63	21.66	15.77
December	0.23	0.62	12.30	1.59	0.52	21.09	8.70